BUTTERWORTH HEINEMANN

Polymer Vol. 36 No. 9, pp. 1817–1825, 1995

0032-3861/95/$10.00+0.00

Electron microscopy and diffraction of crystalline dendrimers and macrocycles*

C. J. Buchko, P. M. Wilson, Z. Xu, J. Zhang, J. S. Moore† and D. C. Martin‡
Materials Science and Engineering, and the Macromolecular Science and Engineering Center, The University of Michigan, 2022 H. H. Dow Building, Ann Arbor, MI 48109-2136, USA
†Department of Chemistry, Roger Adams Laboratory, University of Illinois, Urbana, IL 61801, USA

The precisely defined geometry of phenylacetylene dendrimers and macrocycles makes it possible to investigate systematic variations in chemical architecture on the nature of microstructural organization. Here we report on transmission electron microscopy, selected-area electron diffraction and high-resolution electron microscopy studies of crystalline phases of these synthetic materials. Since the molecules are sensitive to electron beam damage, low-dose techniques were used to capture images and diffraction patterns dynamically. The data show increased crystal misorientation with increasing side-group length and molecular complexity. As the size increases, the number of conformations available to the molecule also increases, making it difficult to pack the molecules with fewer defects.

(Keywords: dendrimer; macrocycle; electron microscopy)

INTRODUCTION

The ability to control explicitly the three-dimensional organization of matter depends upon an understanding of how molecular architecture influences short-range and long-range order. Whitesides *et al.* have outlined strategies for the creation of large molecular assemblies through non-bonded interactions[1]. Weak forces that are directional (like hydrogen bonds) and non-directional (like van der Waals interactions) can result in the spontaneous organization of individual covalently bound molecules into stable systems. One route to self-assembly of organic molecules is the construction of 'shape-persistent', modular units capable of controlling the location and direction of different forces that strongly influence non-covalent interactions. Structural elements that can be used in molecular engineering of shape-persistent units include phenyl rings and acetylene rods.

The two families of molecules used in this study are phenylacetylene dendrimers (PADs) and phenylacetylene macrocycles (PAMs) as seen in *Figure 1*. The PAD series belongs to a specific class of molecules known as dendrimers. Introduced by Tomalia *et al.*[2] with the synthesis of poly(amidoamines), they were first labelled 'starburst' polymers because of their highly branched topology. Generations of the PAD molecule branch out from a seed phenylene in the manner of a tridendron, and contain tertiary butyl groups on the periphery of the molecule to enhance solubility. The unique method for producing these dendrimers involves a repetitive scheme that gives rise to high-molecular-weight molecules in relatively few synthetic steps[3]. The base member of the PAD family is PAD-4 (*Figure 1a*). Chemical routes for dendritic molecules have been developed by other groups[4–7], and some characterization has been undertaken[2,8–10]. Among these studies are structural analysis of molecules in solution[9] and thermal properties of the solid phase[10], but the crystalline forms of low-molecular-weight dendrimers or the structural changes as a function of generation have not yet been evaluated. Recent advances in the large-scale synthesis of poly(propylenimine) dendrimers[11] hold promise for the widespread use of these materials.

The PAM family of molecules is based on a cyclic phenylacetylene backbone (*Figures 1b–d*). The geometry of these molecules and the ability to tailor the length of the side groups creates the potential for many variations. The chemical and physical differences of the side groups attached to the planar base molecule will influence the condensed-phase organization. Planar molecules will often organize in the condensed phase to form nematic and discotic liquid crystals, and are therefore the subject of varied structural analysis techniques. Crystalline and liquid-crystalline structures of disc-like triphenylene monomers have been characterized by Voigt-Martin *et al.*[12] using electron diffraction, high-resolution electron microscopy and molecular simulations. Similar methods have also been used to characterize self-assembling organic nanotubes based on a cyclic peptide architecture[13].

The typical synthesis of a new molecule is time-consuming and yields a small amount of material, often less than a gram. This valuable compound must then be used in several analytical techniques. Single-crystal growth is slow and requires a significant amount of material to prepare a sample suitable for X-ray structure determination. Powder X-ray diffraction

* Presented at 'Aspects of Imaging in Polymer Science', 51st Annual Meeting of the Microscopy Society of America, 1–6 August 1993, Cincinnati, OH, USA

‡ To whom correspondence should be addressed

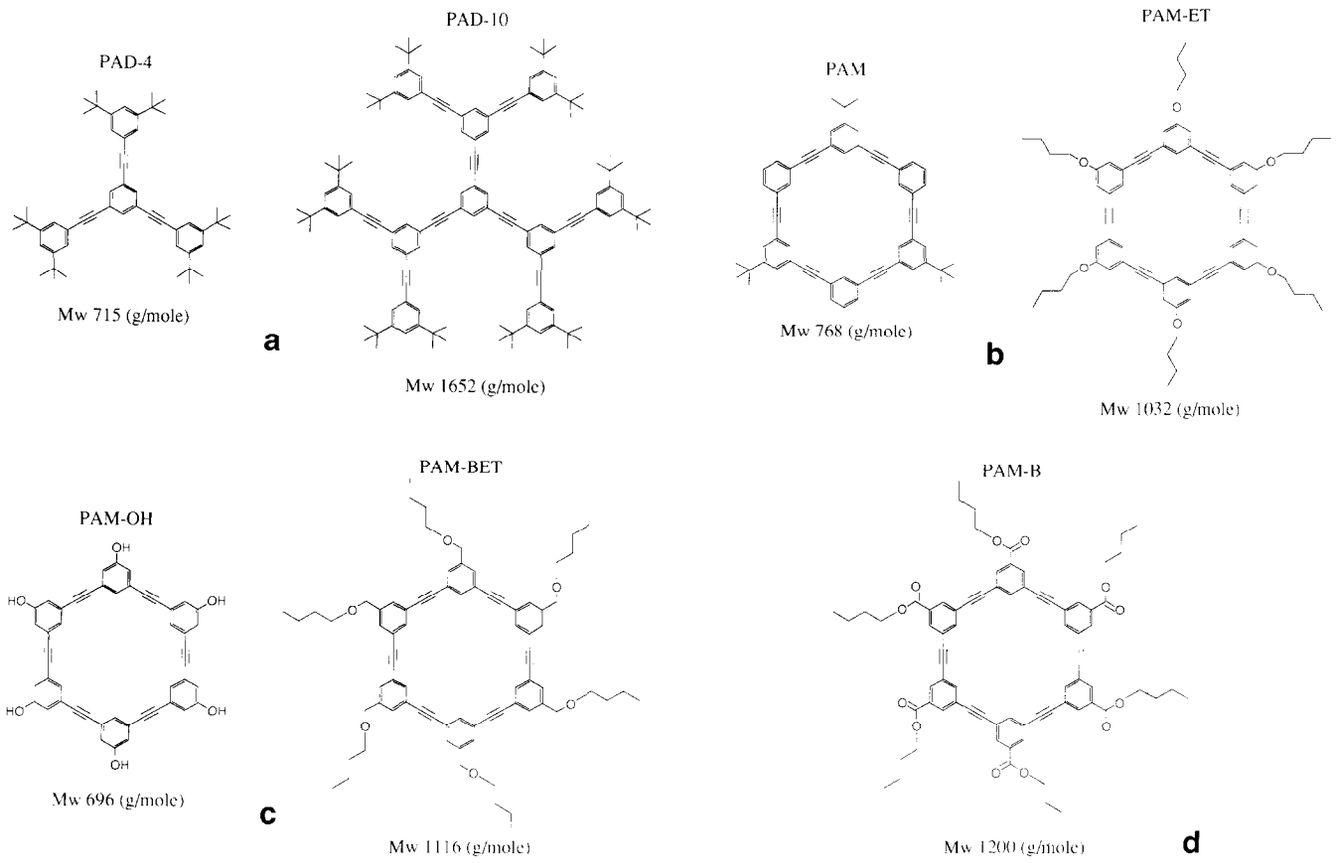

Figure 1 (a) PAD-4 and PAD-10; (b) PAM and PAM-ET; (c) PAM-OH and PAM-BET; (d) PAM-B

patterns (*Figure 2*) of the PAD and PAM families reflect condensed-phase structural changes induced by variations in molecular structure. The PAD series shows a loss of crystallinity with increased size of the molecule. The relationship between condensed-phase order and the different side groups attached to the base PAM molecule is complicated since the groups may vary not only in length but also in chemical composition. Structures with disorder cannot be solved easily by X-ray methods and electron microscopy offers additional information in such systems.

Low-dose selected-area electron diffraction (SAED) and high-resolution electron microscopy (HREM) in conjunction with molecular modelling yield a wealth of structural information from extremely small amounts of sample. This can be used to determine if a particular molecular engineering scheme is giving the desired results. It is also possible to analyse the manner in which processing variations influence the microstructure of the material. Possible applications of these materials include optical waveguides, drug delivery systems, molecular machines, liquid-crystal displays, porous films with well defined pore sizes for filtration, and polymer tubes with one-dimensional transport properties. The success of various approaches to macromolecular engineering depends upon the type of detailed structural information presented here.

TECHNIQUES

The extensive information that can be obtained from low-dose transmission electron microscopy (TEM) makes it a useful tool for structure determination. Since the quantities of these molecules are limited, efficient methods for sample preparation are important. Samples for microscopy generally consist of crystallites deposited from a dilute solution or microtomed samples of bulk crystals. For this study, a dilute solution of the PAM molecules in toluene or the PAD molecules in 50/50 wt% toluene/*N*-methylpyrrolidinone (NMP) solution was deposited onto amorphous carbon-coated mica sheets. The solvent was allowed to dry under normal room conditions. The carbon film and crystallite layer were floated off the mica substrate in deionized water and collected on copper grids. Gold was then evaporated onto the samples at an angle of 10–20° as a calibration standard for electron diffraction studies and to improve contrast at intermediate magnifications. Samples for high-resolution imaging typically are left uncoated, although high-resolution images can also be obtained from coated films. A Reichert–Jung UltraCut E was used to prepare cross-sectional samples of PAD-4 crystals. PAD-4 crystals nucleated from dilute solution on a glass slide were embedded in an epoxy droplet that was then cut and positioned in a larger epoxy block suitable for microtomy.

The primary constraint in the electron microscopy of organic molecules is the effect of the high-voltage electron beams on the sample. The intensity of a particular reflection is given by the following equation[14]:

$$I(D) = I_0 \exp(-J/J_c) + I_\infty$$

where J is the electron dose, I_0 is the intensity at zero dose, I_∞ is the intensity at infinite dose and J_c is the

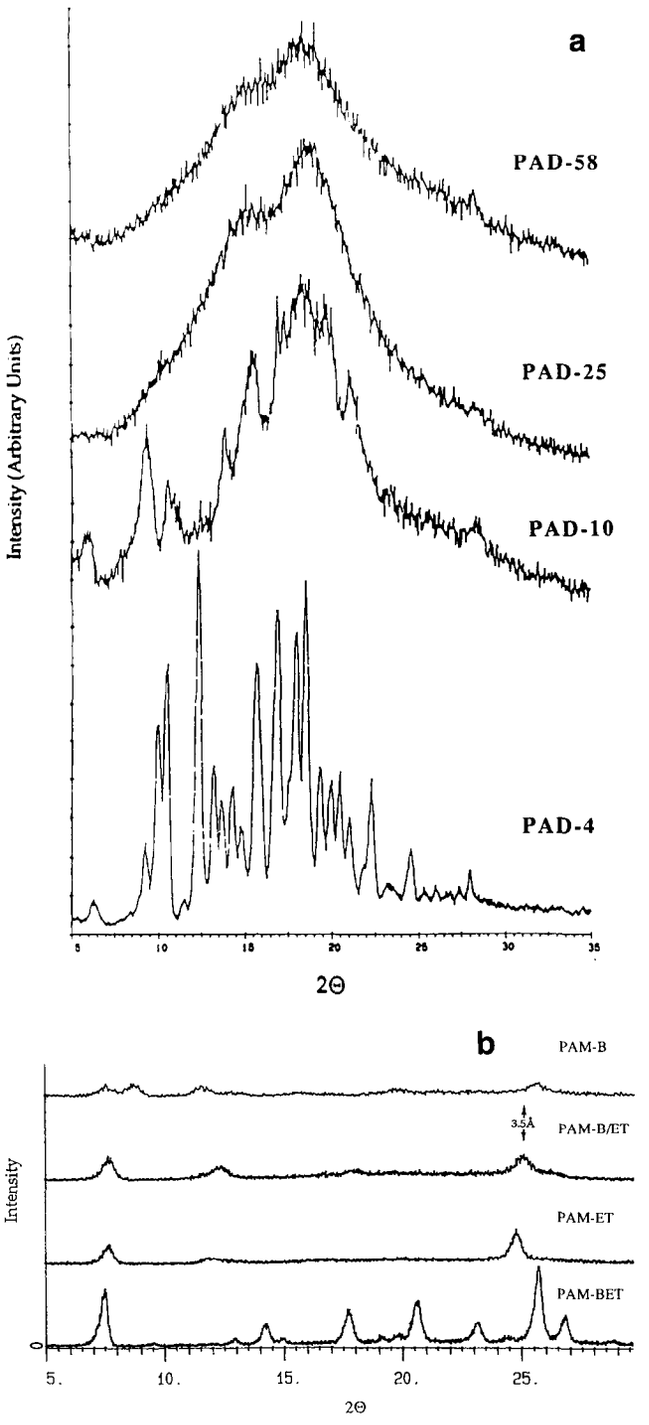

Figure 2 (a) Powder X-ray diffraction patterns for four polyaromatic macrocycle molecules. All the patterns exhibit spacings at approximately 0.35 nm and 1.18 nm. (b) WAXS reveals a continuous loss of crystalline order with each successive PAD generation, indicating the difficulty of packing larger molecules with few defects

critical dose required to reduce the intensity of this reflection by a factor of 1/e. In the laboratory, J_e, the total end-point dose (*TEPD*), is commonly defined as the dose required for a spot to disappear as monitored visually, and estimates of the value of J_e can be made by slow-speed analysis of the video recording. In terms of the operating parameters for low-dose electron microscopy, J_e (C cm^{-2}) is given by the expression:

$$J_e = j_s M^2 t$$

where j_s is the current density at the screen (pA cm^{-2}), M is the magnification and t (s) is the time it takes for the sample to be damaged. *TEPD* was measured for all the samples by monitoring the time needed for a particular reflection to become diffuse and indistinguishable from the amorphous scattering of the carbon film.

For high-resolution electron microscopy of these samples, the operating dose was kept below 85% of the *TEPD* (*Table 1*). Selected-area electron diffraction (SAED) was performed on a JEOL 4000 EX at 400 kV. In order to aid collection of diffraction patterns on materials with a total end-point dose of 10^{-2} C cm^{-2} and lower, a YAG-video system[15] was used in conjunction with an image intensifer and video camera. Data collection was performed by searching the grid at a low dose rate (approximately 10^{-5} C cm^{-2} s^{-1}) while monitoring the video screen and recording the session on VHS tape. Once a suitable sample was found, diffraction patterns were collected either on film or on VHS tape. The images were digitized with a SCION LG-3 frame grabber and analysed with IMAGE 1.47 on a Macintosh Quadra 700. HREM imaging was performed on a JEOL 4000 EX at 400 kV using magnifications from 25 000× to 35 000×. The low magnification allowed these beam-sensitive samples to be imaged at doses less than 10^{-3} C cm^{-2}. Many samples with small lattice spacings are not suitable for imaging at this magnification. In the case of the PAM and PAD families, the lattice spacings were of the order of 2.0 nm, and could be fairly easily resolved.

RESULTS

Phenylacetylene dendrimers

The PAD family of molecules rapidly gain molecular weight with each generation, from first-generation PAD-4 (715 g mol^{-1}) to fifth-generation PAD-94 (14 775 g mol^{-1})[3]. Observation of melting points using differential scanning calorimetry and hot-stage optical microscopy indicate that only the two smallest PAD molecules, PAD-4 and PAD-10, are crystalline. Optical microscopy of PAD-4 crystals nucleating out of solution shows that the crystals appear to have a roughly rectangular cross-section (*Figure 3*). The PAD-10 crystallites used in these microscopy experiments were grown with the same type of toluene/NMP solution used for PAD-4, and have the same general morphology. However, the PAD-10 crystallites are generally smaller (*Figure 4*). Electron micrographs of PAD-4 (*Figure 5*) show long crystals, the aspect ratios of which have been observed to be as high as 40:1. Identical growth conditions generate PAD-10 crystals of the order of 10 μm as opposed to 50 μm for PAD-4. Also, observed aspect ratios of PAD-10 are about five times less than for PAD-4. When samples are prepared out of dilute solution, the crystallite orientation

Table 1 Total end-point dose (C cm^{-2})

PAM	4.5×10^{-2}
PAM-BET	1.8×10^{-2}
PAM-ET	1.4×10^{-2}
PAM-B	8.6×10^{-3}
PAD-4	1.3×10^{-2}
PAD-10	1.2×10^{-3}

Figure 3 OM of PAD-4

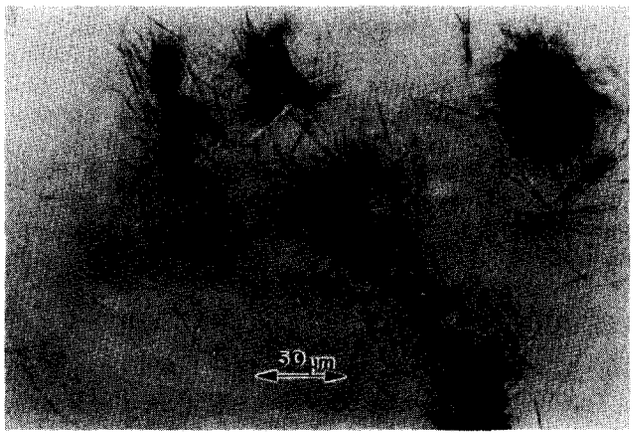

Figure 4 OM of PAD-10

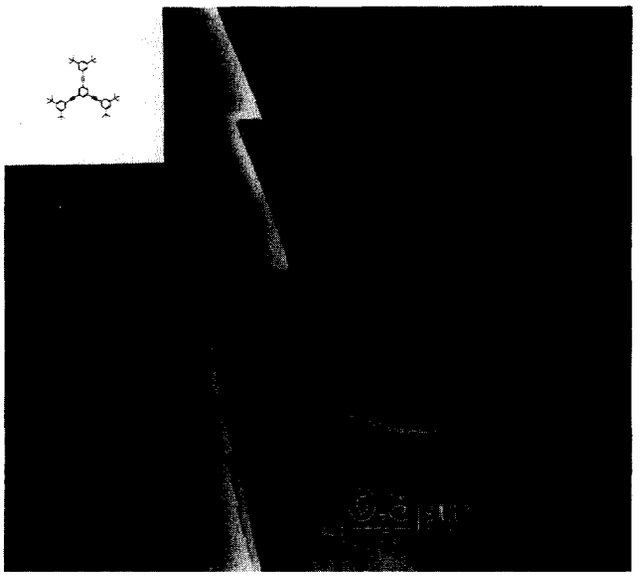

Figure 5 TEM image of PAD-4

allows for analysis of the molecular packing in the long direction of the crystal.

Electron diffraction patterns of PAD-4 (*Figure 6*) reveal characteristic spacings in the long direction of the crystal of 0.64 nm, and a lateral spacing of 2.05 nm, perpendicular to the long direction of the crystal. Electron diffraction from a microtomed cross-section of a PAD-4 crystal (*Figure 7*) shows 2.05 nm and 19.1 nm spacings, with an included angle of 90°. There are no observable systematic absences in the electron diffraction pattern. Diffraction patterns obtained for PAD-10 (*Figure 8*) show a meridional spacing of 0.62 nm. The equatorial dimension is 1.6 nm. *Figure 9* is a high-resolution electron micrograph of the PAD-10 molecule, with lattice fringes of 1.6 ± 0.2 nm.

Phenylacetylene macrocycles

Three forms of the PAM family were investigated in this study: PAM, PAM-ET and PAM-B, as shown in

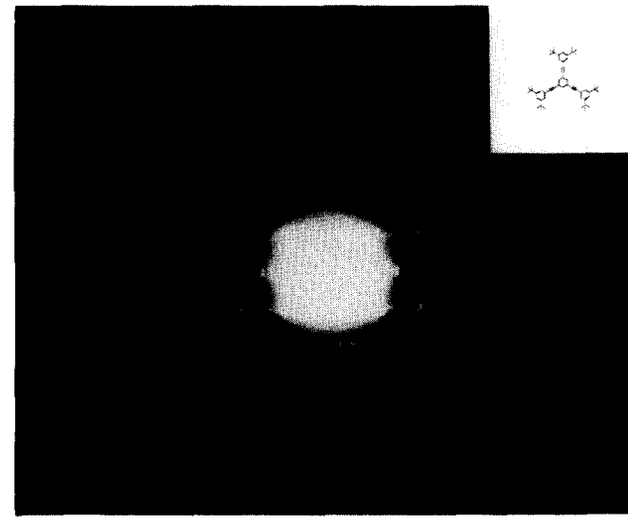

Figure 6 SAED of PAD-4 shows a 0.64 nm spacing alon the *c* axis, and 2.05 nm spacings along the *a* axis

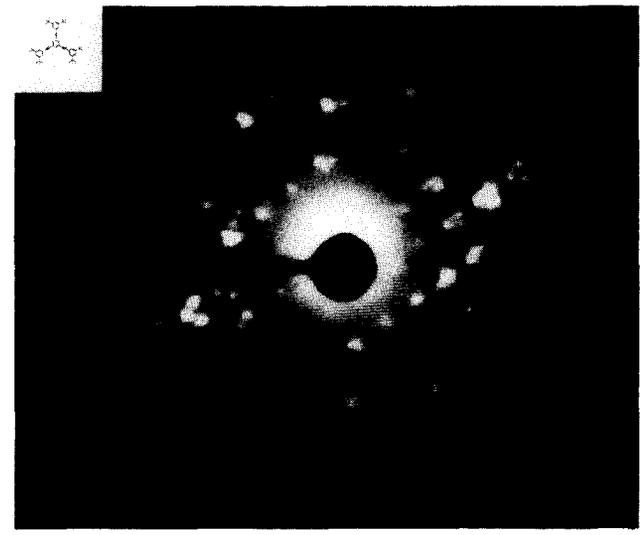

Figure 7 SAED from a cross-section of a PAD-4 crystal. Spacings are 2.05 nm and 19.1 nm, with an included angle of 90°

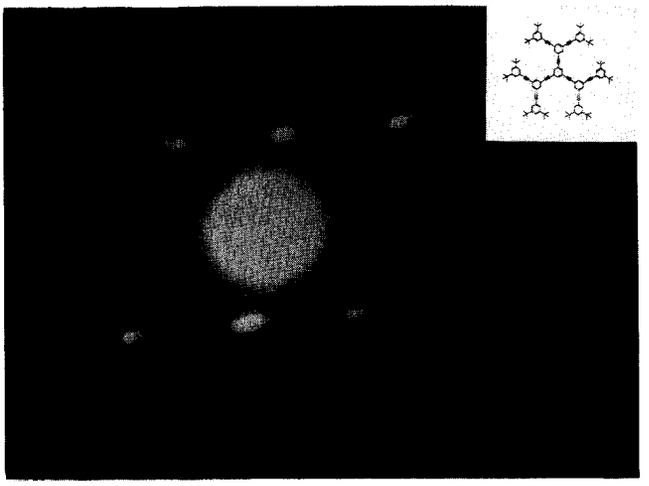

Figure 8 SAED of PAD-10, dynamically captured using low-dose video techniques, has a *c*-axis spacing of ~0.62 nm. Streaking in the *a*-axis direction indicates less order than the three-dimensionally crystalline PAD-4

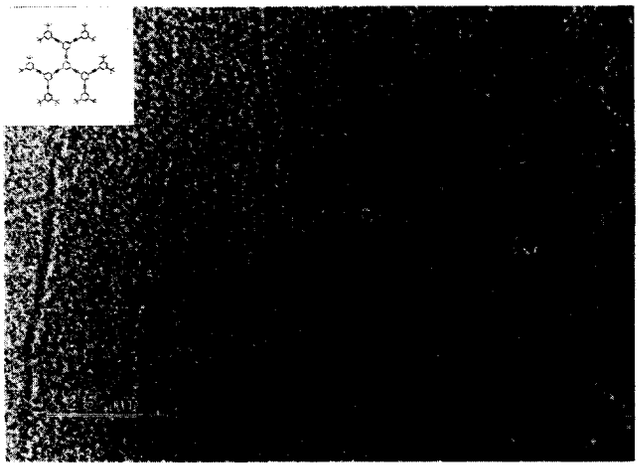

Figure 9 HREM image of PAD-10 with 1.6 ± 0.2 nm lattice fringes labelled. Note the local curvature of the fringes

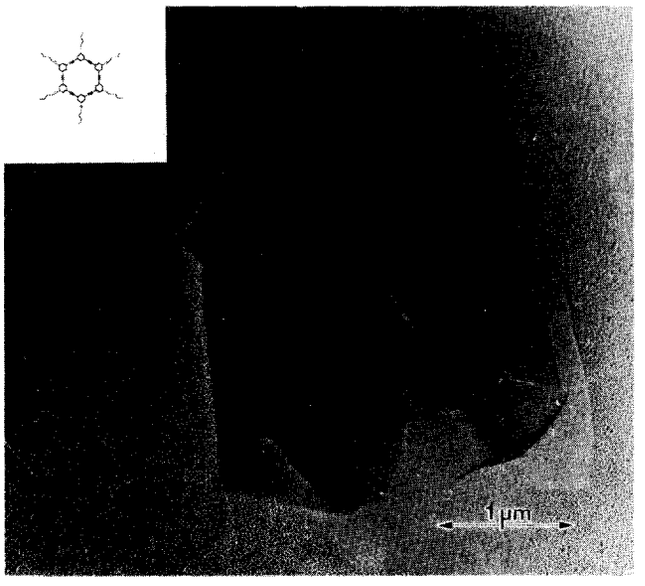

Figure 10 PAM-ET TEM facets, 120°

Figure 1. Transmission electron microscopy showed crystallites of PAM-ET on the substrate. *Figure 10* is a representative crystallite with well defined 120° facets. PAM formed smaller, less well defined crystallites on the substrate. SAED of the PAM crystallites yielded two high-symmetry zone axis patterns, shown in *Figures 11* and *12*. Zone 1 has characteristic spacings of 0.383 nm and 1.090 nm. Zone 2 shows spacings of 0.774 nm and 1.983 nm. Each pattern shows systematic absences, as discussed in more detail in the following section. High-resolution images of PAM-B (*Figure 13*) show crystallites that are misoriented, such that the directions of the lattice fringes can be seen to change orientation (45° or more) over length scales less than 5 nm. The spacings are 2.2 ± 0.2 nm.

DISCUSSION

The PAD family of molecules share a common branched structure emanating from a Y-shaped seed molecule of four phenyl rings joined by acetylene spacers. As in the PAM series, the planarity of the lower-generation molecules gives rise to face-to-face stacking. The 90° angles, yet lack of systematic absences, narrows the unit-cell choices down to simple monoclinic/pseudo-orthorhombic or triclinic, which can be further refined by comparing the relative intensities of simulated diffraction patterns with the observed patterns. *Table 2* is a summary of the proposed unit cell for PAD-4, in which $a = 2.05$ nm, $b = 1.91$ nm, $c = 0.64$ nm, $\alpha = \beta = \gamma = 90°$.

An energy-minimized PAD-4 unit cell (*Figure 14*) shows two interdigitated molecules per unit cell. The rigid, planar PAD-4 molecules pack in a face-to-face manner, with a distance of closest approach of 0.345 nm.

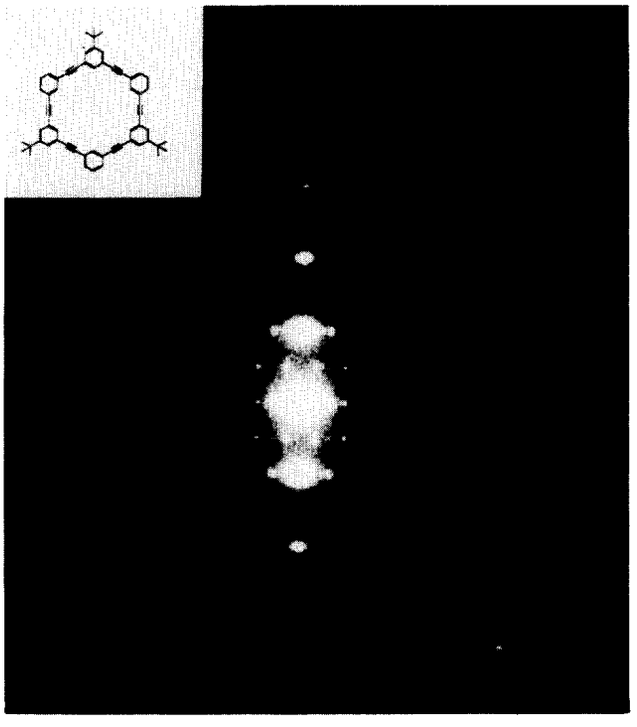

Figure 11 SAED of PAM. Spacings are 0.38 and 1.09 nm. SAED patterns calculated for zone axis [3 1 0] and higher [*h* 1 0] from the hypothesized structure match the experimentally observed pattern

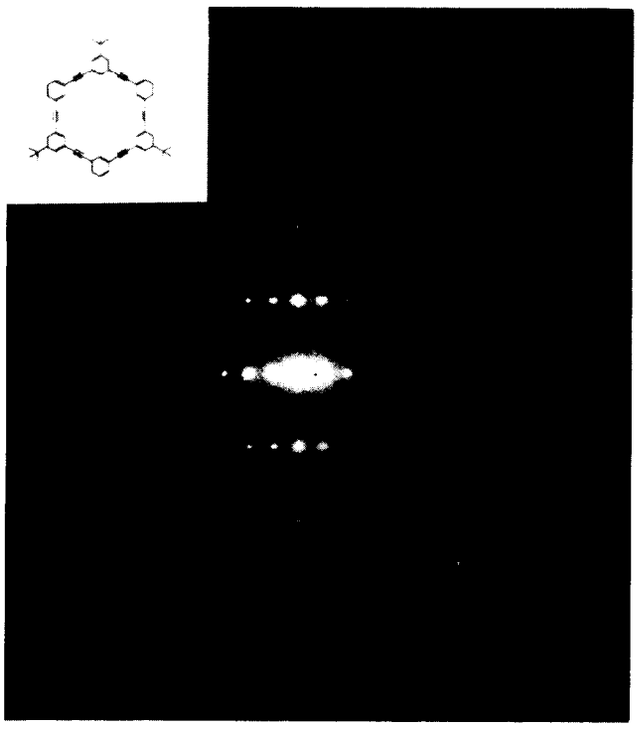

Figure 12 SAED of PAM crystal. Spacings are 0.77 and 1.98 nm

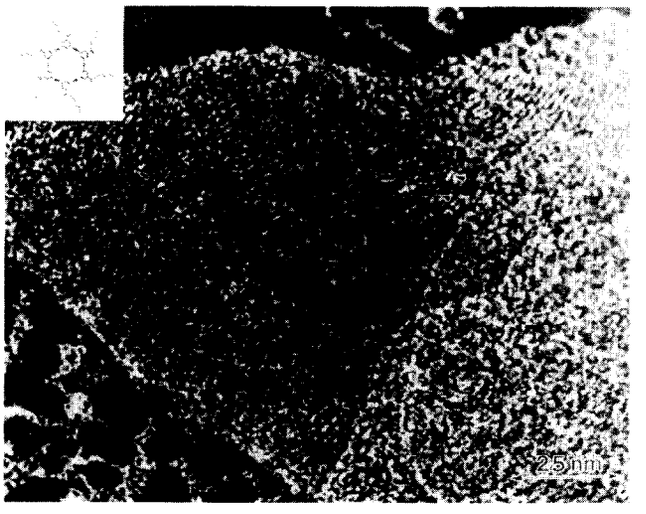

Figure 13 HREM image of gold-shadowed PAM-B films, which show 2.2 ± 0.2 nm fringes. The crystallites (arrows) change directions significantly (45° or more) over short distances (less than 5 nm)

However, the geometric axis of each PAD-4 is tilted at approximately a 66° angle with respect to the *c* axis. This conformation was predicted by analysis of the possible spatial relationships of two molecules in the proposed unit cell, and confirmed by the elimination of bad contacts and energy minimization. Further support for this configuration comes from the strong (5 0 1) reflection in the PAD-4 diffraction patterns, which corresponds to a real-space dimension of 0.35 nm, the distance of closest approach for these planar molecules. The tilted nature of the stacks is responsible for the weak reflections along the (0 0 1) axis in both the experimental and simulated patterns. The off-axis projection of the PAD-4 unit cell (*Figures 15a* and *15b*) better illustrates the stacks of molecules, and *Figure 15c* shows the (0 0 1) projection of the two molecules in the unit cell.

Electron diffraction patterns of PAD-10 resemble those of PAD-4 in that there are more high-order equatorial reflections than layer lines. Also, the scattering vector perpendicular to the long axis of the crystal, taken as reciprocal vector $\boldsymbol{k}_1$, extends farther out in reciprocal space than $\boldsymbol{k}_2$, the scattering vector along the long axis of the crystal, such that the ratio of $k_2/k_1 = 0.6$. Both of these observations indicate greater order perpendicular to the long axis of the crystal than parallel, in both PAD-4 and PAD-10. The lower *TEPD* and fewer reflections of PAD-10 as compared to PAD-4 corroborate the trend of decreasing crystallinity with increasing molecular complexity revealed in WAXS of the PAD family. Further information about the structure of PAD-10 is available from the HREM images. The orientation of the crystallites used to image the lattice fringes indicates that this 1.6 ± 0.2 nm dimension corresponds to the side-to-side packing of tilted stacks of molecules.

The PAM molecules are built on a ring structure, often with a two-, three-, or six-fold symmetry to the molecule depending on the side groups attached to the phenyl rings. This common symmetry is seen when observing the crystallites grown from dilute solution of PAM-ET. The crystallites have 120° facets and the SAED pattern of these crystals shows a minimum of three-fold symmetry. Since the crystallites exhibit symmetry that is present in the molecule, it may be possible to assume that the molecules are rigid and maintain their symmetry when packing. This observation is borne out

Table 2 Proposed PAD-4 unit cell (determined by SAED and WAXS)

Crystal system	Monoclinic/ pseudo-orthorhombic or triclinic
Space group	P2 or P1
a (nm)	2.05
b (nm)	1.91
c (nm)	0.64
$\alpha = \beta$ (deg)	90
γ (deg)	90
Density, calc. (g cm^{-3})	0.941
Density, obsd. (g cm^{-3})	0.988

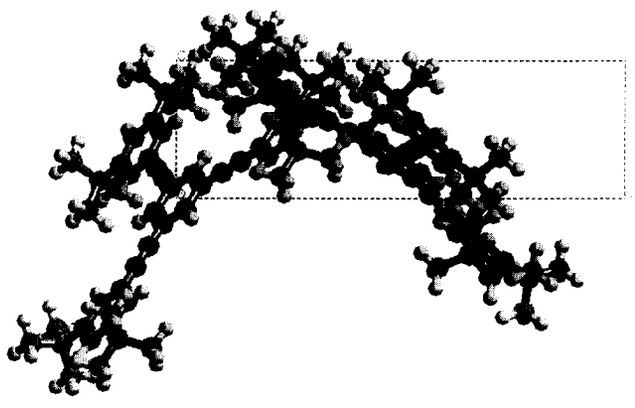

Figure 14 The (0 1 0) projection of the proposed PAD-4 unit cell with monoclinic/pseudo-orthorhombic symmetry. Note the interdigitation of the Y-shaped molecules

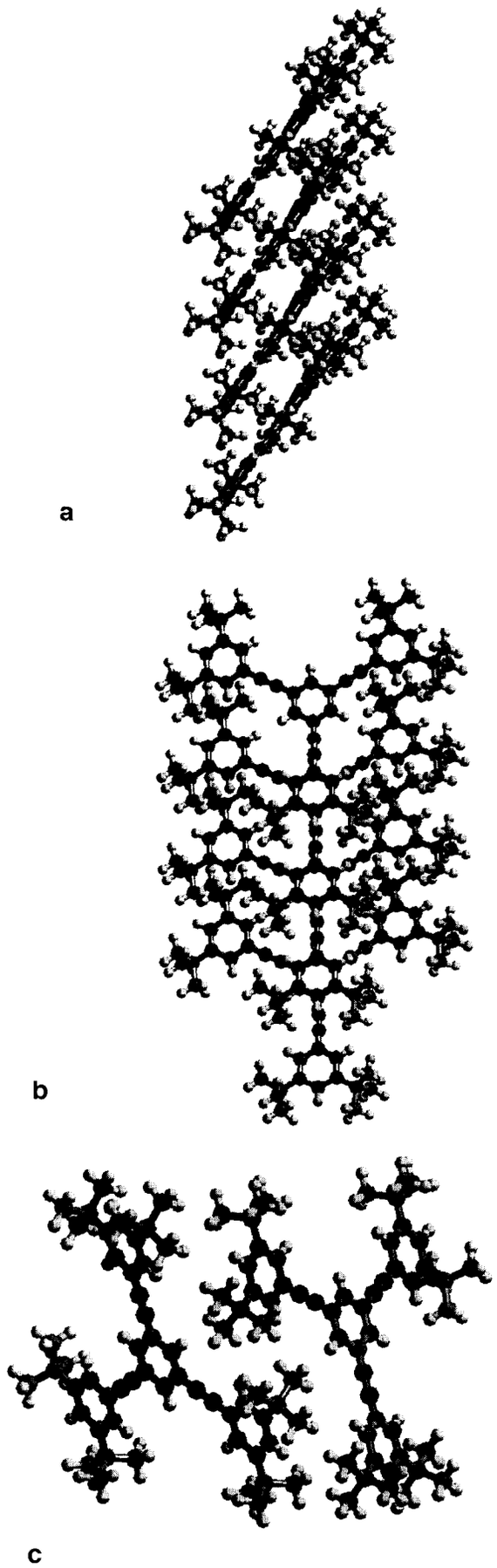

Figure 15 (a) and (b) The 0.35 nm face-to-face packing of the PAD-4 molecules can be observed in these two off-axis projections. (c) The (0 0 1) view of the molecular arrangement in the unit cell

by molecular simulation of a single PAM molecule. Molecular dynamics of isolated molecules performed using Polygraf[16] show that the deviations from the planar structure conformation are small. The inherent rigidity of the phenyl groups with the acetylene spacers tends to keep the molecule ring rigid. If two molecules were brought together in a face-to-face manner, the distance of closest approach without having bad contacts is 0.35 nm. This planarity could give rise to packing of the molecules as 'discs', similar to the PAD-4 structure.

A quantitative analysis of the electron diffraction patterns taken from the molecules provides structural information that can be used to rule out certain unit cells. *Figures 11* and *12* are electron diffraction patterns of two zone axes of the PAM crystals. The two patterns show the following systematic absences of reflections. If the pattern in *Figure 11* is assumed to be the $0\,k\,l$ zone, then absences are $(0\,0\,l)$ where l are odd. The 0.383 nm spacing of the layer lines corresponds to the possible face-to-face packing of the molecules. The additional SAED pattern, *Figure 12*, can be indexed as the $h\,l$ zone with absences of $(h\,0\,l)$ where l is odd. The spacings (0 0 2) and (1 0 0) are 0.774 nm and 1.983 nm, respectively. Additional support for a hypothesis where the molecules stack in a face-to-face manner is found in the intensity of the $(0\,0\,l)$ spots where l is even. The systematic absences limit the choices of the space groups for the unit cell to $P112_1$ or $P6_3$. The three-fold symmetry of the molecule fits neatly into a hexagonal unit cell, thereby minimizing bad contacts. The calculated SAED patterns from the proposed structure shown in *Table 3* match the experimental patterns well in intensity and absences as shown in *Figure 16*. While further refinement of the unit cell is anticipated as more information becomes available, the current best fit to the experimental data is a $P6_3$ space group ($a=b=2.235$ nm, $c=0.774$ nm, $\alpha=\beta=90°$, $\gamma=120°$) with the motif being one-third of the PAM molecule as seen in *Figure 17*.

Further support of the hexagonal unit-cell hypothesis is found in the structure determined for PAM-OH by X-ray crystallography[17]. A single crystal of PAM-OH was solution-grown over a three-month period[18], and conventional X-ray crystallography provided a unit cell with space group $P3_2$ (*Figure 18* and *Table 4*). The PAM-OH structure is similar to the proposed PAM structure, with one important difference. The stacks of PAM-OH molecules are shifted by the presence of the hydroxide groups, which want to participate in hydrogen bonding, whereas the PAM molecules stack directly on top of each other, with a 30° rotation around the geometric z-axis of each molecule, to accommodate the

Table 3 Proposed PAM unit cell (determined by electron diffraction)

	1	2
Crystal system	Monoclinic/ pseudo-hexagonal	Hexagonal
Space group	$P112_1$	$P6_3$
a (nm)	2.235	2.235
b (nm)	2.235	2.235
c (nm)	0.774	0.774
$\alpha=\beta$ (deg)	90	90
γ (deg)	120	120
Density, calc. (g cm^{-3})	0.763	0.763
Density, obsd. (g cm^{-3})	0.95	

bulky butyl groups. This periodicity can be clearly seen in the (1 0 0) and (0 0 1) projections of the proposed crystal structure for PAM (*Figure 17*). The free volume in the structure of the PAM-OH unit cell makes it possible for the crystallites to retain up to 28% solvent by weight. This solvent uptake might account for the disparity between the observed density measurement of 0.95 g cm^{-3} for PAM crystals and the calculated density of the

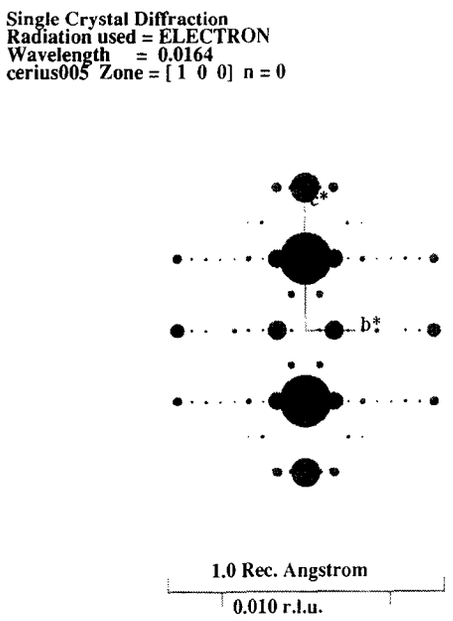

Figure 16 Simulated diffraction pattern of PAM using CERIUS software

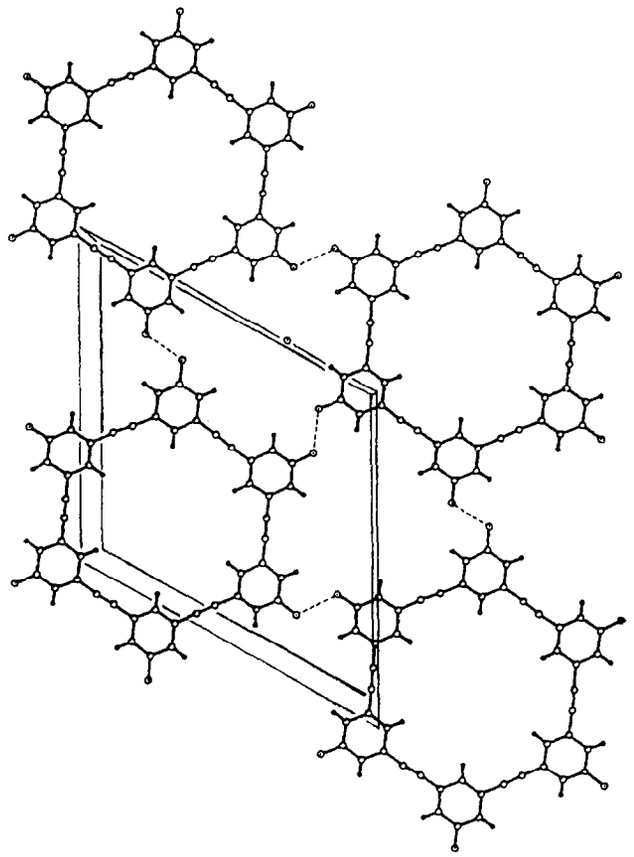

Figure 18 The crystal structure of PAM-OH has been solved by conventional single-crystal X-ray diffraction. The structure confirms that the PAM molecules can pack face-to-face in a triclinic or hexagonal unit cell

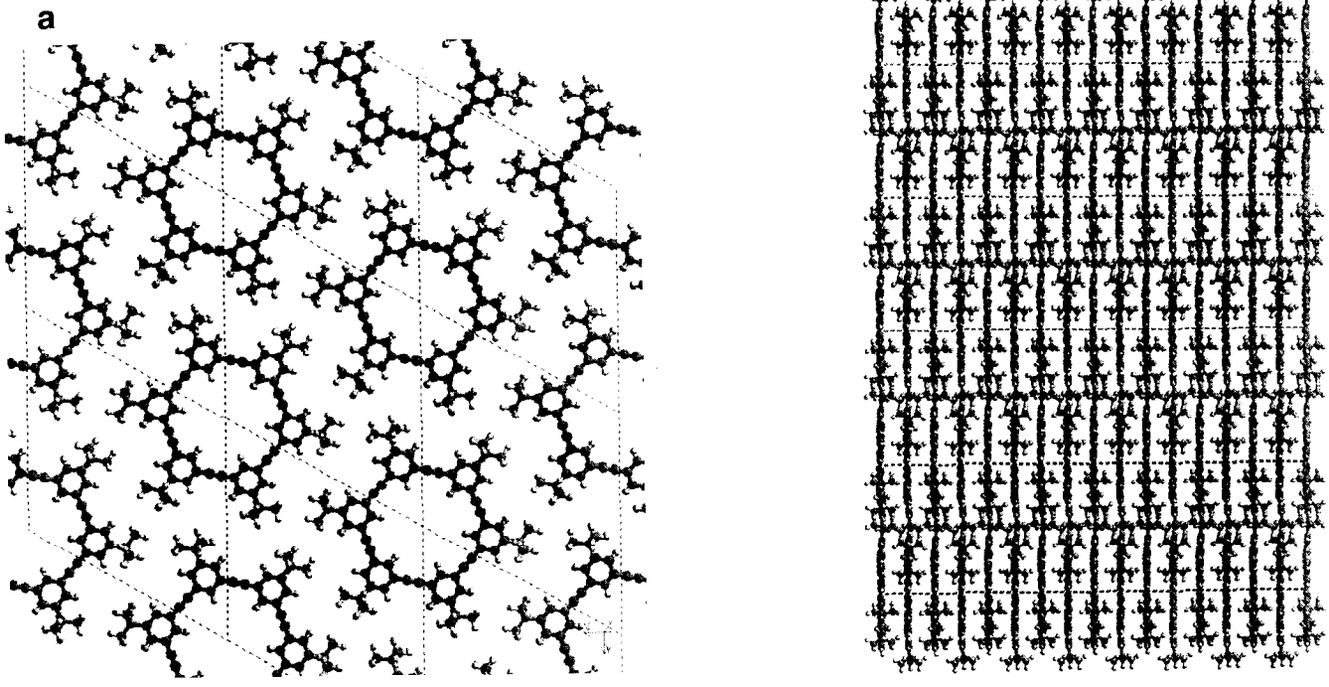

Figure 17 (a) The (1 0 0) projection of proposed crystal structure for PAM. The apparent extra three t-butyl groups on each PAM are actually from the second layer of molecules. (b) The (0 0 1) projection of proposed crystal structure for PAM

Table 4 PAM-OH unit cell (determined by single-crystal X-ray diffraction[17])

Crystal system	Trigonal
Space group	$P3_2$
a (nm)	2.0659
b (nm)	2.0659
c (nm)	0.9997
$\alpha = \beta$ (deg)	90
γ (deg)	120
Density, calc. (g cm^{-3})	1.29
Density, obsd. (g cm^{-3})	1.24

proposed structure, 0.763 g cm^{-3}. The observed density of the PAM molecule was measured from a solution-grown crystal, allowing solvent incorporation in the structure.

PAM-B molecules form thin, non-uniform films as seen by contrast from gold shadowing. Thin regions of this film were ideal for high-resolution imaging at low doses. The images reveal that the molecules do not pack together easily, as in the PAM molecule. The crystallites are misoriented, such that the directions in the lattice fringes can be seen to change orientation (45° or more) over length scales less than 5 nm. The fringes are 2.2 ± 0.2 nm, corresponding to the side-to-side packing of stacks of PAM-B molecules. Additionally, the lattice fringes show other defects, like edge dislocations, illustrating the difficulty of packing these larger molecules as side-group complexity is increased. This direct observation of the packing of the PAM family of molecules correlates well with the observed trend of solution aggregation and formation of liquid-crystalline phases due to chemical side-group manipulation.

CONCLUSIONS

In general, the findings of this study corroborate previous observations that the crystallinity decreases as the molecular complexity of the PAD series increases. A unit cell for PAD-4 in which the molecules orient themselves as tilted stacks has been identified. For the PAM family, the data obtained by electron microscopy and other structural probes suggest that these macrocycles organize in a face-to-face manner, and that the unit cell for two forms may have a three- or six-fold symmetry. Different solid-phase structures of the PAM series have been identified, along with possibilities for liquid-crystalline phases. These two families of molecules share a characteristic face-to-face packing distance of about 0.35 nm, owing to the 'distance of closest approach' of the aromatic groups. This information describes a preferential planar orientation of individual molecules in the condensed phase that can be modified by the chemical composition and physical conformation of groups appended to aromatic substructures.

ACKNOWLEDGEMENTS

PMW would like to thank the Air Force for a AFOSR fellowship. DCM and JSM would also like to thank NSF for National Young Investigator Awards. This work is sponsored by NSF grant CHE-9202095, the Michigan Memorial Phoenix Project, the College of Engineering, the 3M Company and the Petroleum Research Fund.

REFERENCES

1 Whitesides, G. M., Mathias, J. P. and Seto, C. T. *Science* 1991, **254**, 1312
2 Tomalia, D. A., Baker, H., Dewald, J., Hall, M., Kallos, G., Martin, S., Roeck, J., Ryder, J. and Smith, P. *Polym. J.* 1985, **17** (1), 117
3 Xu, Z. and Moore, J. S. *Angew. Chem., Int. Edn. Engl.* 1993, **32** (2), 246
4 Newkome, G. R., Yao, Z., Baker, G. R. and Gupta, V. K. *J. Org. Chem.* 1985, **50**, 2003
5 Hawker, C. J. and Frechet, J. M. *J. Chem. Soc., Chem. Commun.* 1990, 1010
6 Mekelburger, H. B., Jaworek, W. and Voegtle, F. *Angew. Chem. Int. Edn. Engl.* 1992, **31** (12), 1571
7 Zhou, L. L. and Roovers, J. *Macromolecules* 1993, **26** (5), 963
8 Smith, P. B., Martin, S. J., Hall, M. J. and Tomalia, D. A. 'Applied Polymer Analysis and Characterization' (Ed. J. Mitchell), Hanser, Munich, 1987, pp. 357–85
9 Briber, R. M., Bauer, B. J., Hammouda, B. and Tomalia, D. A. *Polym. Mater. Sci. Eng.* 1992, **67**, 430
10 Wooley, K. L., Hawker, C. J., Pochan, J. M. and Frechet, J. M. J. *Macromolecules* 1993, **26** (7), 1514
11 de Brabander-van den Berg, E. M. M. and Meijer, E. W. *Angew. Chem. Int. Edn. Engl.* 1993, **32** (9), 1308
12 Voigt-Martin, I. G., Garbella, R. W. and Schumacher, M. *Macromolecules* 1992, **25**, 961
13 Ghadiri, M. R., Granja, J. R., Milligan, R. A., McRee, D. E. and Khazanovich, N. *Nature* 1993, **366**, 324
14 Kumar, S. and Adams, W. W. *Polymer* 1990, **31**, 15
15 Liao, J. and Martin, D. C. *Science* 1993, **260**, 1489
16 Molecular Simulations Inc., Burlington, MA, 1993
17 Structure solved by S. Lee, Department of Chemistry, University of Michigan
18 Zhang, J. Ph.D. Dissertation, University of Michigan,1993